

Wideband Monitoring of FRB 180916.J0158+6 Across a Half-Decade Bandwidth Using the Upgraded GMRT

SIDDHARTHA BHATTACHARYYA,¹ JAYANTA ROY,¹ AND APURBA BERA²

¹*National Centre for Radio Astrophysics, Tata Institute of Fundamental Research, Pune, 411007, India*

²*International Centre for Radio Astronomy Research (ICRAR), Curtin University, Bentley, WA 6102, Australia*

ABSTRACT

With the uGMRT having unprecedented sensitivity and unique capability of providing instantaneous frequency coverage of 250–1460 MHz, we studied FRB 180916.J0158 + 65 over four months sampling during its active phase. We report the detection of 74 bursts at Band-3 (i.e. 250–500 MHz) and 4 bursts at Band-4 (i.e. 550–750 MHz) of uGMRT providing a burst rate of ~ 4 bursts/hour above a fluence of 0.05 Jy ms. We find that the source emits maximum energy and luminosity up to a fractional bandwidth of 70 MHz near the middle of its activity window consistent with earlier studies. We see a strong correlation between the excess dispersion measure and excess scattering width where both of them attains their maximum value near the middle of the activity window. We find that the normalized cumulative distribution of the waiting time can be well-fitted by an exponential function, indicating a stochastic emission process. We also notice that the cumulative burst rate changes rapidly with the intrinsic energy of the bursts near the middle of the activity window considering the full observed window of 0.4-0.6 of this FRB, where this change is much steeper for the high-energy bursts and shallower for the low-energy bursts.

Keywords: methods: observational – techniques: transients; fast radio bursts.

1. INTRODUCTION

Fast radio bursts (FRBs) are short-duration, bright, dispersed radio pulses of yet unknown physical origin (Rajwade & van Leeuwen 2024). For FRBs, the dispersion measure (DM) values are typically 5 to 20 times larger than the Milky Way’s contribution to the observed DMs (DM_{MW}), implying that FRBs are extragalactic in origin and located at cosmological distances, corresponding to a redshift range of 0.09–3.5 (Rajwade & van Leeuwen 2024). For more details about the physical properties of FRBs, the reader may refer to the review articles (eg. Petroff et al. 2019). Several emission models (e.g. Zhang 2023) involving progenitors from cosmic strings to compact objects have been proposed to explain all the bursts originating from the sources but none of them gives us a clear picture to date. One of the main challenges behind the difficulties in constraining the origin of the FRBs is that, in most cases, they are one-off events, exhibiting a single millisecond burst of radio emission.

More than 800 FRBs have been reported to date¹. Approximately 55 FRBs have been found to repeat, with multiple bursts recorded from a single source, leading them to be labelled as “repeaters.” Till now only 2 repeaters, *viz.* FRB 20121102A and FRB 20180916B have shown periodicity in their activities (Braga et al. 2024; Andersen et al. 2019). Further, out of 55 repeaters detected to date, only 18 events were localised with their associated host galaxies (refer to <https://www.frb-hosts.org/>). On the other hand, the majority of detected FRBs (> 800) are events, where only a single burst has been observed from each source. However, it is not clear whether the progenitors of repeaters have different physical origins compared to those of one-off events. Moreover, the detection of ~ 500 times fainter bursts from FRB 20171019 (Kumar et al. 2019) compared to the originally detected burst suggests that the identification of the repeating nature of an FRB may strongly depend on instrumental sensitivity. Also, the spectra of many repeaters are not well constrained due to the lack of appropriate beam shape information in some cases (e.g. Connor et al. 2020). Considering those facts there

Corresponding author: Siddhartha Bhattacharyya
sbhattacharyya@ncra.tifr.res.in, sid.phy.in@gmail.com

¹ <https://www.wis-tns.org/>

is a possibility that all FRBs are repeaters (Caleb et al. 2019), and for the one-off, the less sensitive follow-up failed to detect the fainter repeating bursts from the same FRB.

Over the past decade, most FRBs have been detected over a frequency range of 110 MHz to 8 GHz (e.g. Pleunis et al. 2021a, Bethapudi et al. 2023) with the only few events from FRB 20121102A also being detected in the 4–8 GHz frequency range (Gajjar et al. 2018). Though FRB emission extends to lower frequencies, only a few FRB searches were conducted below the frequency of 400 MHz (e.g. Deneva et al. 2016, Rajwade et al. 2020, Pastor et al. 2021, Pilia et al. 2020).

Observations of FRBs at low frequencies are important to check whether there is any intrinsic cutoff or turnover frequency in their emission, which could provide valuable insights into their progenitor models (e.g. Houben et al. 2019). It also may happen that FRBs are undetectable at low frequencies due to (a) spectral turnover arising from propagation effect (e.g. Chawla et al. 2020), and/or (b) multi-path propagation of signals in the intervening medium which is a phenomenon called as scattering (e.g. Ocker et al. 2022). The facts mentioned above are useful to constrain the properties of circumbursts medium of an FRB detected at low-frequency (e.g. CHIME/FRB-Collaboration et al. 2020, Ravi et al. 2019). Moreover, the frequency-dependent activity of FRBs (Pleunis et al. 2021a) can also be studied using the observations at low frequencies.

The CHIME/FRB-Collaboration et al. 2021 reported the detection of a relatively bright repeater FRB 180916.J0158 + 65, which is denoted here as FRB 20180916B. Later Marcote et al. 2020 localized this repeater and found its host galaxy using the European VLBI Network (EVN) taking advantage of its repeating nature. They found that this repeater is located in a nearby massive star-forming spiral galaxy at a distance of ~ 150 Mpc ($z \approx 0.03$), where this galaxy has ~ 100 times larger stellar mass and ~ 5 times higher metallicity compared to the dwarf host galaxy associated with the FRB 20121102A (Marcote et al. 2020). Further, no persistent radio source with flux density $> 18 \mu\text{Jy}$ at 1.6 GHz (Marcote et al. 2020), has been seen at the location of this FRB which implies that if any persistent radio emission is associated with this repeater then its luminosity is a few hundred times lower than that of the persistent source coincident with other repeaters, say FRB 20121102A (Marcote et al. 2017). Andersen et al. 2019 reported the detection of 28 bursts from this repeater over a time span of ~ 400 days and they estimated periodicity of ~ 16.35 days in the repetition pattern of this FRB with an active window of ~ 4 days.

The average burst rate of this repeater within the active window is ~ 1.8 burst per hour above fluence limit of 5 Jy ms (CHIME/FRB-Collaboration et al. 2020), however, this rate is lower towards the edge in comparison to the centre of the active window (e.g. Marcote et al. 2020). Later Chawla et al. 2020 reported detection of this FRB emission up to 110 MHz using simultaneous observations with a few partial overlapped bands at LOFAR (110–190 MHz), GBT (300–400 MHz) and CHIME (400–800 MHz). They also placed a lower limit of the spectral index of this repeater is $\alpha > -1$. Recently, Bethapudi et al. 2023 reported the detection of eight bursts from this FRB 20180916B using the 100-m Effelsberg radio telescope with frequency range 4–8 GHz. They found clear evidence of chromaticity, as the activity window of this repeater shifts with frequency. The bursts detected at ~ 6 GHz (Bethapudi et al. 2023) are narrower in time, wider in frequency, and exhibit lower fractional bandwidths compared to bursts at lower frequencies. Additionally, the burst rate varies with frequency as $f^{-2.6 \pm 0.2}$, and it also differs from cycle to cycle, with the spectral index estimated from the rate–frequency relation being -1.04 ± 0.08 (Bethapudi et al. 2023).

Previously Marthi et al. 2020 reported the detection of 15 bursts from this repeater using the upgraded Giant Metrewave Radio Telescope (uGMRT) over a frequency range of 550–750 MHz. They observed these bursts over three successive cycles of approximately 2 hours each, during the peak of its expected active period. The burst rate was found to be highly variable, with the faintest burst being only about 10 times brighter than the brightest Galactic burst detected to date. They did not detect any persistent radio source associated with this repeater and placed a 3σ upper limit on the persistent radio flux density of $66 \mu\text{Jy}$ at 650 MHz. Further, Sand et al. (2022) and Trudu et al. (2023) used the uGMRT to observe this repeater over a frequency range of 250–500 MHz, detecting four and seven bursts, respectively. In addition to the above mentioned observations, recently Bethapudi et al. (2024) reported 116 bursts from this repeater using uGMRT over a frequency range of 550–750 MHz.

Here we report the detection of low-frequency radio bursts from FRB 20180916B with the uGMRT over a frequency range of 250–750 MHz. Section 2 discusses the details of the observation and data analysis. In Section 3, we present our findings on the variation of physical parameters of the detected bursts from this repeater. Finally, we discuss and summarize our key findings in Section 4.

2. OBSERVATION AND DATA ANALYSIS

The energy emitted from an FRB can vary significantly with frequency, highlighting the importance of investigating its emission across a wide frequency range. For FRB 20180916B, in addition to the CHIME (600 MHz) where the repeater FRB 20180916B had been first observed, several other telescopes, viz. LOFAR (150 MHz), uGMRT (650 MHz), SRT (328 MHz), GBT (350 MHz), Apertif (1370 MHz), Effelsberg (1420 MHz), EVN (1700 MHz) etc, detected bursts from this repeater. Interestingly there is almost no existing observation with a single telescope which probed the bursts over an instantaneous wide frequency range. The current uGMRT observation presented in this paper utilises the wide bandwidth capabilities of uGMRT (Gupta et al. 2017) to observe FRB 20180916B simultaneously at 250 – 500 MHz (Band-3), 550 – 850 MHz (Band-4) and 1060 – 1460 MHz (Band-5) respectively.

2.1. Observation

The uGMRT (Gupta et al. 2017) is an interferometric array of 30 parabolic dishes each with 45m in diameter. We observed with phased array beams pointed at the position of FRB 20180916B, i.e. RA = 01^h58^m00^s.75 and DEC = 35°43′00″.75 (Marcote et al. 2020), in seven epochs over the period from 26th November 2020 (MJD = 59179) to 21st March 2021 (MJD = 59294). The multi-subarray observing capability of the uGMRT enabled us to simultaneously form three phased array beams, one at each band – Band-3 (having a usable band of 250 – 500 MHz), Band-4 (having a usable band of 550 – 850 MHz) and Band-5 (having a usable band of 1060 – 1460 MHz) – covering a wide frequency range of 250 – 1460 MHz. This multi-subarray observing mode splits the full interferometric array of 30 dishes into three sub-arrays of 10 dishes each, which gave us the 10 σ theoretical fluence sensitivity of 0.21, 0.46 and 0.38 Jy ms for Band-3, Band-4 and Band-5 respectively, where to estimate these values we have considered the maximum scattered pulse for both Band-3 and Band-4 and for Band-5 we have assumed the scattering width of 1 ms. Each of the phased array beams was recorded in 8192 frequency channels with ~ 48.83 kHz frequency resolution and 655.36 μ s time resolution.

2.2. Data Processing

The phased array total intensity data with ~ 48.83 kHz frequency resolution and 655.36 μ s time resolution from each sub-array, were processed in the same manner. We used the GMRT Pulsar Tool named as

*GPTOOL*² to perform mitigation of radio frequency interference (RFI). We generated RFI-cleaned *SIGPROC* (Lorimer 2011) filterbank file for further processing. The data were then incoherently dedispersed (Lorimer & Kramer 2005) to correct for the dispersion caused by the cold ionised plasma in the intervening medium, including the interstellar medium (ISM) of the Milky Way, the host galaxy of the source, and the intergalactic medium (IGM). We performed the above-mentioned incoherent dedispersion using the *prepsubband* tool, which is a part of the software *PRESTO*³, for a *DM* range of 340 – 360 pc cm⁻³ with *DM* step of 0.01 pc cm⁻³. We then searched for the FRB pulses using *single_pulse_search.py* tool of *PRESTO* above a signal-to-noise (*S/N*) threshold of 5 with an upper limit of pulse width as 65.536 ms (i.e. up to box-car of 100 bins). The lowering of the threshold reduces the chance of missing the band-limited bursts from the repeating FRB. We identified the genuine bursts by manually examining the pulsed emission pattern (potentially band-limited) in the dynamic spectrum and the bow-tie structure in the DM-time plane. We performed this feature extraction of every detection using *your_candmaker* which is a tool of the software package *your*⁴. We identified a total of 74 bursts from FRB 20180916B observed at Band-3, only 4 bursts from at Band-4 and no bursts from Band-5. However, we did not find any simultaneous detections in Band-3 and Band-4. Out of 74 bursts detected at Band-3, 26 bursts were detected with $6.5 \leq S/N < 7$, 22 bursts were detected with $7 \leq S/N < 10$ and 26 bursts were detected with $S/N > 10$ whereas in Band-4 all the four bursts were detected with $S/N > 7$. For further statistical analysis of burst morphology and FRB parameters, we focus on the bursts detected in Band-3, i.e. a total of 74 bursts with $S/N \geq 6.5$.

2.3. Activity Phase

Previously several studies (e.g. Chawla et al. 2020) reported the activity period of this repeater which is ~ 16.35 days with an active window of ~ 4 days. We have folded the MJDs of the observation epochs and found the phase (ϕ) of each detected burst from this repeater using the relation

$$\phi = \frac{T - T_0}{P} - \text{int} \left(\frac{T - T_0}{P} \right) \quad (1)$$

where T is the MJD of the bursts, $T_0 = 58369.18$ (Chawla et al. 2020) is the starting MJD and $P = 16.35$

² <https://github.com/chowdhuryaditya/gptool>

³ <https://github.com/scotttransom/presto>

⁴ <https://github.com/thepeabyteproject/your>

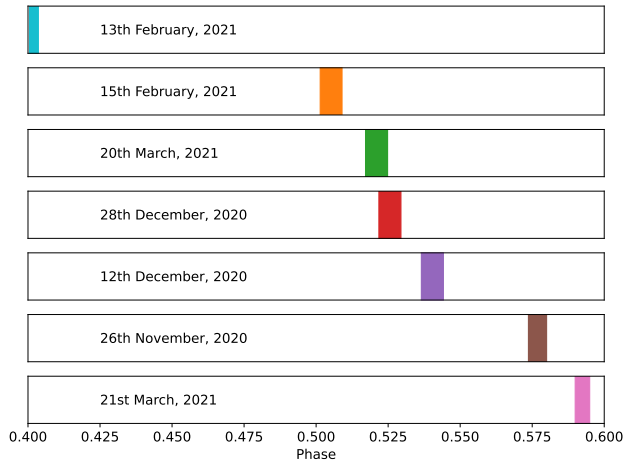


Figure 1. The phase space sampling of FRB 20180916B was conducted using approximately 18 hours of total uGMRT observations, divided across seven different epochs.

days (Chawla et al. 2020) is the activity period of FRB 20180916B. Figure 1 shows the phase values (eq. 1) covered in each observation epoch discussed earlier. Out of total ~ 18 hours of total observation duration (splits into seven different epochs), around 12 hours observation time (splits into four different epochs) sampled the activity phase of this repeater over a phase range of ~ 0.51 to ~ 0.55 whereas the full observation duration sampled the phase space from $\phi \simeq 0.4$ to $\simeq 0.6$. However, these observations did not uniformly sample the phase space of this repeater within the phase range $0.4 \leq \phi \leq 0.6$, where Figure 1 shows a large discontinuity in the phase sampling from $\phi \simeq 0.4$ to $\phi \simeq 0.5$.

The phase range covered by each of the observation epochs is tabulated in table 1. Furthermore, we have not tested the active window of this repeater because the observations referenced above did not cover the repeater’s full phase space. We have estimated the phase value of all the detected bursts from this repeater using Eq. 1 and examined how the physical parameters of the bursts change with their phase values, which is discussed later in this paper.

By combining all seven epochs, we sampled the activity phase of FRB 20180916B from approximately 0.4 to 0.6 (Table 2), although this phase space sampling was not continuous. It has been reported that the activity phase of this repeater depends on the observing frequency (Pastor et al. 2021). Therefore, we consider only other observations with frequency ranges comparable to our observing bands. These observations include GBT (300 – 400 MHz) (Chawla et al. 2020), CHIME (400 – 800 MHz) (Mckinven et al. 2023; Pearlman et al. 2020; Sand et al. 2022), SRT (300 – 400 MHz) (Trudu

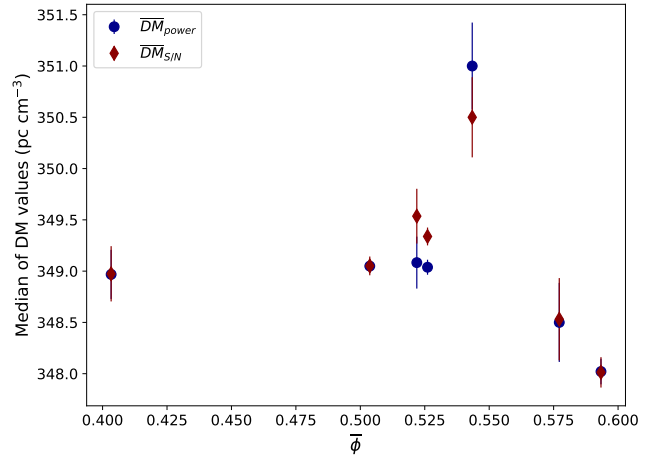


Figure 2. The variation of the median value of power optimised DM (\overline{DM}_{power}) and S/N optimised DM ($\overline{DM}_{S/N}$) with the median value of activity phases ($\bar{\phi}$) of FRB 20180916B at each of the observation epochs. Here the error bars show the uncertainty in the estimation of \overline{DM}_{power} , $\overline{DM}_{S/N}$ and $\bar{\phi}$.

et al. 2023), and previous uGMRT (300 – 500 MHz) observations (Sand et al. 2022; Trudu et al. 2023). These studies sampled the activity phase of FRB 20180916B from approximately 0.37 to 0.65 (Table 2), which is nearly equivalent to our sampling range.

2.4. Power Optimised DM

The *single_pulse_search* algorithm (discussed earlier) gives us an approximate value of DM of the pulse which further needs a correction depending on the maximization of either the S/N or the power of the detected pulse, where the detection process focuses on enhancing the detectability of the burst by maximising the contrast between the signal and the background noise using S/N -optimised DM , for studying the intrinsic properties of the burst one needs to preserve the signal’s total energy by power-optimised DM . First, we discuss the estimation of DM depending on maximising the S/N value. During the detection process, we have de-dispersed the detected pulse with different search- DM values and estimated their S/N values. We then fit the S/N values of the pulse for different DM s with a Gaussian function and estimate the correct DM for which the S/N is maximum which is called the S/N -optimised DM . We now discuss the estimation of DM that depends on the power of the pulse, which is called power-optimized DM . For this task, we have used the method presented by Lin et al. 2022. (Lin et al. 2022) takes the input of a filterbank file (often known as a dynamic spectrum) of a burst which is already de-dispersed at S/N -optimised DM . Then this burst is decomposed into Fourier modes

along the time axis and the modes are independently fitted with a correct DM . After that DM values from different Fourier modes are combined into a single measurement using optimal weighting schemes and estimated the optimal DM of that burst. The entire process has been repeated for N number of trials and recorded the optimal DM values at each trial which is then used to determine the uncertainty in the final DM value by taking the standard deviation of a sample of optimal DM values obtained at different trial.

We considered studying the median value per scan of both power-optimized DM , denoted as \overline{DM}_{power} and S/N -optimized DM , denoted as $\overline{DM}_{S/N}$ with the median value of activity phases ($\overline{\phi}$) of this repeater covered at different observation epochs. The blue and red points of figure 2 show the variation of \overline{DM}_{power} and $\overline{DM}_{S/N}$ of the detected bursts with $\overline{\phi}$ of FRB 20180916B. We find that for most of the cases the values of \overline{DM}_{power} and $\overline{DM}_{S/N}$ are almost similar and only for a few cases do they have a very small difference. This is quite obvious as for most of the detected bursts presented in this paper we have single component profiles for which power-optimized DM and S/N -optimized DM are almost equal and they are widely differed for the multi-component profile and drifted pulse, which is merely present in the sample of 74 detected bursts mentioned earlier. However, from now and onwards, we use power-optimized DM as the measured DM values of these 74 bursts detected at Band-3 of uGMRT. The range of power-optimized DM values of the detected bursts for each of the observation epochs is tabulated in table 1.

Combining all seven observing epochs, the DM values of the 74 bursts from this repeater lie within the range of $341.24 - 356.71$ pc cm $^{-3}$. However, the DM values reported from other observations (Table 2) lie within the range of $347.3-370.4$ pc cm $^{-3}$, which overlap with the DM values from our observations, including the detection of a few bursts with lower DM values.

2.5. Profile and Spectra

We will now discuss the profile and spectra fitting of the detected bursts. The middle panel of figure 3 shows the colour scale plot of the filterbank file, commonly known as waterfall diagram, of a detected burst, where the X-axis is time of the observation and Y-axis is the frequency of the observation. The signal is present in band-3 of the uGMRT starting from 300 MHz. The colour gradient of the waterfall diagram (figure 3) shows the intensity of the burst in the frequency-time plane. On the upper and right panels we have the profile of that burst by averaging over the frequency and the spectra of that burst by averaging over the time duration re-

spectively. The estimated profile and spectra have been shown in the red lines of the upper and right panels of the figure 3 respectively.

The pulse profile of the burst is fitted with a Gaussian function convolved with an exponential tail, which is given by

$$I_P(t) = A_P \exp\left(-\frac{t - \mu_P}{\tau}\right) \text{Erfc}\left(-\frac{t - \mu_P - (\sigma_P^2/\tau)}{\sigma_P\sqrt{2}}\right) \quad (2)$$

where, $I_P(t)$ is intensity of the pulse profile for a given time t , and the fitting parameters A_P , μ_P , σ_P and τ are determined by the least square method. We have estimated the intrinsic and scattering widths of a burst using Eq. 2. The parameter $\sigma_P \times 2 \ln 2$ gives us the intrinsic width (w_{int}) of the pulse for which the intensity of the pulse is dropped by 50% of its peak value and the parameter τ gives us the scattering width respectively. The blue dashed line in the upper panel of figure 3 shows the fitting of the pulse profile using Eq. 2. The range of intrinsic and scattering width of the detected bursts for each of the observation epochs is tabulated in table 1.

Across all seven observing epochs, the intrinsic and scattering widths of the 74 bursts from this repeater range from 0.68 to 29.53 ms and 0.03 to 14.47 ms, respectively (Table 2). Since both intrinsic and scattering widths depend on observing frequency, we only consider detections from this repeater reported in the literature within frequency ranges similar to our observing band (*i.e.*, 250 – 500 MHz). These include CHIME (400 – 800 MHz) (CHIME/FRB 2020; Pearlman et al. 2020; Sand et al. 2022), GBT (300 – 400 MHz) (Chawla et al. 2020), SRT (300 – 400 MHz) (Trudu et al. 2023), and previous uGMRT observations in the 300 – 500 MHz range (Sand et al. 2022; Trudu et al. 2023). The reported intrinsic widths from these observations range from 0.58 to 23.0 ms, which almost overlap with the intrinsic widths observed in our study, where we detected some broadened pulses from FRB 20180916B. In contrast, only Chawla et al. (2020) and Sand et al. (2022) have reported the scattering width values for bursts from this repeater using GBT (300 – 400 MHz) and previous uGMRT (300 – 500 MHz) observations. Their reported values, ranging from 1.67 to 5.90 ms (table 2), partially overlap with our observations, where we detected more scattered pulses from FRB 20180916B.

The spectrum of the burst has been fitted with a Gaussian function, expressed as

$$I_S(f) = A_S \exp\left(-\frac{(f - \mu_S)^2}{2\sigma_S^2}\right) \quad (3)$$

where, $I_S(f)$ is intensity of the spectra for a given frequency f , and the fitting parameters A_S , μ_S and σ_S

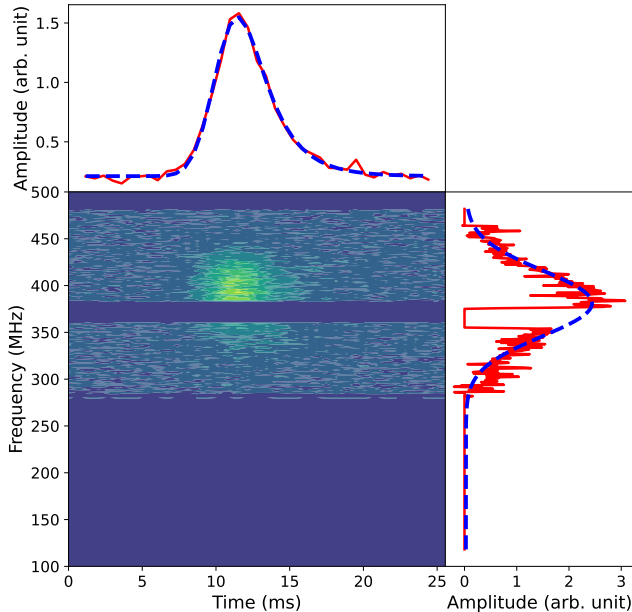


Figure 3. The dynamic spectrum (middle panel), profile (upper panel) and spectra (right panel) of a burst from FRB 20180916B detected at Band-3 of uGMRT.

are determined by the least square method. We have estimated the peak frequency and band occupancy of a burst using Eq. 3. The parameter μ_S gives us the peak frequency (ν_{peak}) of the burst which is a frequency value where the intensity of the spectra is maximum. The parameter $\sigma_S \times 2 \ln 2$ gives the band occupancy (ν_{band}) of the burst for which the intensity is dropped by 50% of its peak value. The blue dashed line in the right panel of figure 3 shows the fitting of the spectra using eq. 3. The range of peak frequency of the detected bursts for each of the observation epochs is tabulated in table 1.

Across all seven observing epochs, the measured values of ν_{peak} and ν_{band} were found to range 311.84 – 475.53 MHz and 48.75 – 121.88 MHz, respectively. However, no such information is available in the existing literature related to FRB 20180916B.

3. RESULTS

In this section, we explore the variation of the physical parameter with the activity phase of FRB 20180916B depending on the 74 bursts detected from this repeater using Band-3 of uGMRT. We estimated the median values of the physical parameters and activity phases of this repeater across different observation epochs, with the goal of improving the modeling of the source mechanism and the local environment of the FRB.

3.1. Flux Density and Intrinsic Fluence

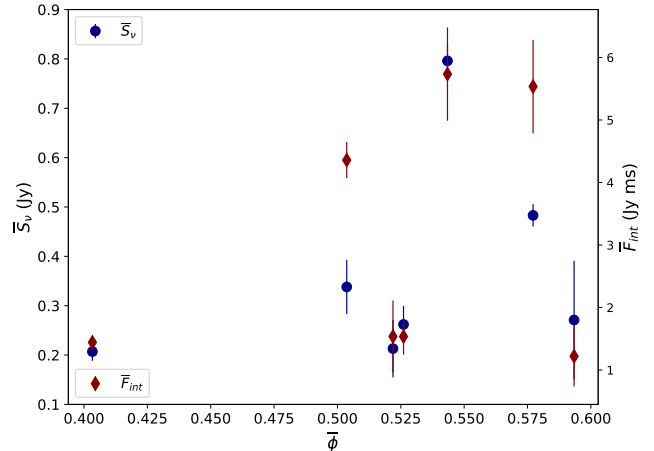


Figure 4. The variation of median values of flux density (\bar{S}_ν) and intrinsic fluence (\bar{F}_{int}) with the median value of activity phases ($\bar{\phi}$) of FRB 20180916B at each of the observation epochs. Here the error bars show the uncertainty in the estimation of \bar{S}_ν , \bar{F}_{int} and $\bar{\phi}$.

We estimated the flux density (S_ν) of each of the bursts detected at Band-3 of uGMRT using the calibrator 3C48 (Ott et al. 1994), which was observed along with FRB 20180916B at each observation epoch. We consider here the median value of flux density, denoted as \bar{S}_ν , instead of their actual values for each of 74 detected bursts and study its variation with $\bar{\phi}$. The blue points of figure 4 show the variation of \bar{S}_ν with $\bar{\phi}$ of FRB 20180916B, which peaks its maximum value at $\bar{\phi} = 0.54$. This implies the source of this repeater emits its maximum luminosity near the middle of its activity window since the host galaxy of FRB 20180916B is localised and its comoving distance is fixed. The range of flux densities of the detected bursts for each of the observation epochs is tabulated in table 1.

Across all seven observing epochs, the flux densities of the 74 bursts from this repeater range from 0.12 to 2.40 Jy (Table 3). Since flux density strongly depends on the observing frequency, we only consider earlier detections with observing frequencies comparable to our observing band (*i.e.*, 250 – 500 MHz). These include CHIME (400 – 800 MHz) (CHIME/FRB 2020; Pearlman et al. 2020; Sand et al. 2022), GBT (300–400 MHz) (Chawla et al. 2020), SRT (300–400 MHz) (Trudu et al. 2023), and previous uGMRT (300 – 500 MHz) observations (Sand et al. 2022; Trudu et al. 2023). The reported flux densities from these studies range from 0.3 to 12.2 Jy (Table 3), which partially overlap with the flux density values of FRB 20180916B obtained from our observations, where we detected fainter bursts from this repeater.

Table 1. The range of observed and derived parameters of the 74 bursts detected at Band-3 of uGMRT. The symbols DM , w_{int} , τ , S_ν , F_{int} and ν_{peak} stand for dispersion measure (power optimized), intrinsic width, scattering width, flux density, intrinsic fluence and peak frequency respectively.

Observable Parameters	Epochs						
	13Feb2021	15Feb2021	20Mar2021	28Dec2020	12Dec2020	26Nov2020	21Mar2021
Duration (hour)	1.5	3	3	3	3	2.5	2
Phase range	0.401 – 0.404	0.501 – 0.509	0.517 – 0.525	0.522 – 0.529	0.537 – 0.544	0.574 – 0.580	0.590 – 0.595
No. of bursts	3	7	27	9	5	14	9
DM range (pc cm ⁻³)	348.54 – 352.05	347.87 – 349.45	345.30 – 356.71	348.96 – 350.50	341.24 – 354.41	342.13 – 350.31	346.94 – 351.90
w_{int} range (ms)	4.56 – 7.80	4.07 – 14.25	0.68 – 28.34	0.83 – 9.50	2.22 – 16.41	3.89 – 29.53	0.72 – 15.10
τ range (ms)	0.15 – 0.22	0.40 – 9.78	0.03 – 4.61	0.04 – 14.47	1.55 – 11.52	0.18 – 1.40	0.05 – 0.31
S_ν range (Jy)	0.17 – 0.38	0.21 – 1.10	0.12 – 1.17	0.15 – 0.85	0.64 – 1.07	0.30 – 0.76	0.16 – 2.40
F_{int} range (Jy ms)	1.33 – 1.73	1.34 – 6.30	0.14 – 13.42	0.18 – 4.63	2.11 – 13.07	1.45 – 15.23	0.21 – 8.61
ν_{peak} range (MHz)	361.86 – 379.04	325.11 – 449.48	311.84 – 475.53	334.18 – 445.21	409.61 – 440.24	315.10 – 454.90	327.22 – 392.02

We estimated the intrinsic fluence (F_{int}) of this repeater (represents the intrinsic energy emitted by the source) by multiplying the flux density (S_ν) of each bursts with its intrinsic width (w_{int}) getting from the profile fitting discussed in the previous section. We considered here the median value of the intrinsic fluence, denoted as \overline{F}_{int} , similar to \overline{S}_ν and study its variation with $\overline{\phi}$. The red points of figure 4 show the variation of \overline{F}_{int} with $\overline{\phi}$ of FRB 20180916B. We find that the variation of \overline{F}_{int} with $\overline{\phi}$ follows a particular nature, where it peaks its maximum value at $\overline{\phi} = 0.54$. This implies the source of this repeater emits its maximum intrinsic energy (E_{int}) near the middle of its activity window since the host galaxy of FRB 20180916B. The range of intrinsic fluence of the 74 detected bursts for each of the observation epochs is tabulated in table 1.

Across all seven observing epochs, the intrinsic fluence of the 74 bursts from this repeater ranges from 0.14 to 15.23 Jy ms (Table 3). Similar to flux density, intrinsic fluence also depends on the observing frequency, so we consider only earlier detections with observing frequencies comparable to our observing band (*i.e.*, 250 – 500 MHz). These include the same observations previously mentioned for flux density. The reported fluence from these studies ranges from 0.4 to 172 Jy ms (Table 3), with the intrinsic fluence values from our observations being a subset of this range, where we detected more bursts with lower intrinsic fluence from FRB 20180916B.

For each of the detected bursts, we estimate the value of F_{int} from the corresponding value of S_ν using the relation $F_{int} = w_{int} \times S_\nu$, where w_{int} has been estimated separately using profile fitting and no dependency on the value of S_ν . However, the variation of median values

of intrinsic width (\overline{w}_{int}) with $\overline{\phi}$, which is not shown in this paper, has similar characteristics as we have seen in the variation of \overline{S}_ν with $\overline{\phi}$. As a result, combining the variations of \overline{S}_ν and \overline{F}_{int} with $\overline{\phi}$ (figure 4), it shows that both of \overline{S}_ν and \overline{F}_{int} peak at the same value of $\overline{\phi} = 0.54$. This implies that the source FRB 20180916B emits its maximum energy and luminosity near the middle of its activity window, which has not been reported in the existing literature on this FRB 20180916B.

3.2. Excess DM and Scattering Width

The value of DM gives us the integral electron column density whereas the value of τ gives us the nature of turbulence along the line-of-sight of the observation. Several studies (e.g. Bhat et al. 2004) find the correlation between the DM and τ for Galactic pulsars. However, no such correlation has been found between DM and τ for extragalactic pulses such as FRBs.

We now consider the excess value of \overline{DM}_{power} (discussed in Section 2.4), defined as $\overline{\Delta DM}_{power} = \overline{DM}_{power} - \overline{DM}_{power}(\overline{\phi} = 0.6)$. Similarly, we consider the median value of the scattering width per scan, denoted by $\overline{\tau}$, and define the excess value of $\overline{\tau}$ as $\overline{\Delta \tau} = \overline{\tau} - \overline{\tau}(\overline{\phi} = 0.6)$. In other words, we study the excess values of both \overline{DM}_{power} and $\overline{\tau}$ relative to their minimum values observed at $\overline{\phi} = 0.6$. The values of $\overline{\Delta DM}_{power}$ and $\overline{\Delta \tau}$ are expected to exhibit evolution intrinsic to the source and/or its local environment.

Figure 5 shows the variation of $\overline{\Delta DM}_{power}$ and $\overline{\Delta \tau}$ with $\overline{\phi}$. We observe that both $\overline{\Delta DM}_{power}$ and $\overline{\Delta \tau}$ reach their maximum values at $\overline{\phi} = 0.54$. Additionally, these two parameters exhibit similar characteristics, showing a correlation with a Pearson correlation coefficient of 0.9. However, this type of qualitative relationship between

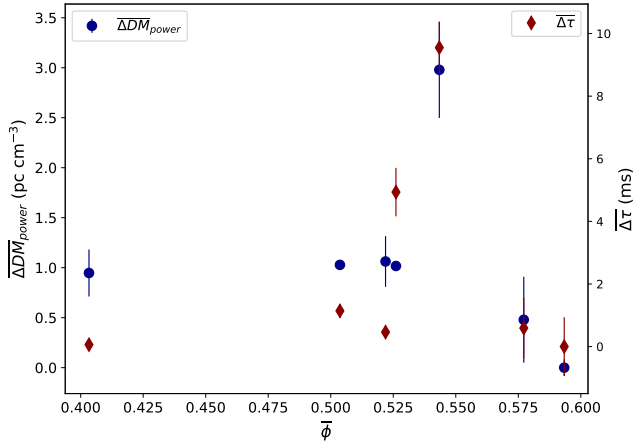


Figure 5. The variation of median values of excess power optimized DM ($\overline{\Delta DM}_{power}$) and excess scattering width ($\overline{\Delta w_{sc}}$) with the median value of activity phases ($\bar{\phi}$) of FRB 20180916B at each of the observation epochs. Here the error bars show the uncertainty in the estimation of $\overline{\Delta DM}_{power}$, $\overline{\Delta w_{sc}}$ and $\bar{\phi}$.

$\overline{\Delta DM}_{power}$ and $\overline{\Delta \tau}$ has not been reported in the existing literature on FRB 20180916B.

3.3. Peak Frequency and Band Occupancy

FRB 20180916B have been observed across a wide range of radio frequencies from 110 MHz to 8 GHz (table 3). The peak frequency (ν_{peak}) of a burst observed detected in the uGMRT observation gives us the frequency at which its energy maximises, where the intrinsic frequency is different by a constant factor of $(1+z)$.

Further the detected bursts show a “band-limited” structure, where the emission is strong in a limited frequency range, named as emission bandwidth (ν_{band}) of the burst. In section-2.5 we discussed how we arrived at the estimated value of ν_{peak} and ν_{band} using the spectra fitting of a burst (following Eq. 3). Here we discuss the variation of the median values of ν_{peak} per scan (denoted as $\bar{\nu}_{peak}$) and ν_{band} (denoted as $\bar{\nu}_{band}$), with $\bar{\phi}$ of FRB 20180916B at each of the observation epoch.

Figure 6 shows the variation of $\bar{\nu}_{peak}$ and $\bar{\nu}_{band}$ with $\bar{\phi}$ of this repeater. We find that the variation of both $\bar{\nu}_{peak}$ and $\bar{\nu}_{band}$ with $\bar{\phi}$ have some definite characteristic, where $\bar{\nu}_{band}$ attains its minimum value at $\bar{\phi} = 0.54$ and $\bar{\nu}_{peak}$ peaks its maximum value at the same $\bar{\phi}$. This implies that the source FRB 20180916B performs an emission with the highest emission frequency (within the observation bandwidth of the telescope) when it reaches near the middle of its activity window. However, this qualitative nature of $\bar{\nu}_{peak}$ could improve the modeling of the emission characteristics of this repeater.

3.4. Waiting Time

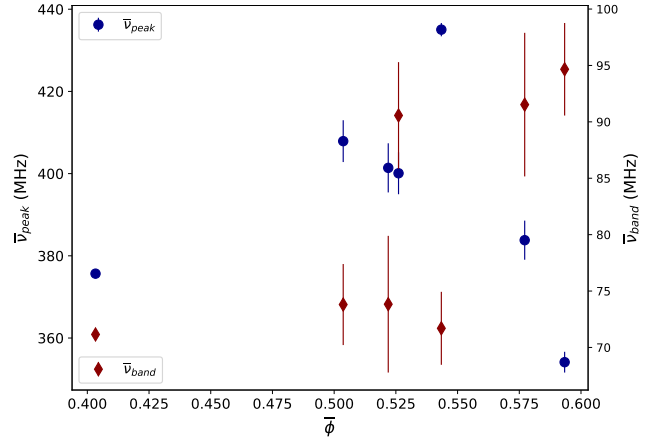


Figure 6. The variation of median values of peak frequency ($\bar{\nu}_{peak}$) and band occupancy ($\bar{\nu}_{band}$) with the median value of activity phases ($\bar{\phi}$) of FRB 20180916B at each of the observation epochs. Here the error bars show the uncertainty in the estimation of $\bar{\nu}_{peak}$, $\bar{\nu}_{band}$ and $\bar{\phi}$.

The arrival time of a burst is obtained from the single_pulse_search tool which gives the candidate time (T_{cand}) by setting the clock to zero at the start of each scan of each observation epoch. For each of the observation epochs, the burst waiting time (T_{wait}) is estimated by considering the T_{cand} difference between two consecutive bursts. We have repeated this process for all other observation epochs separately.

The study of waiting time distribution is crucial for understanding the physical nature of the source. The normalized cumulative burst rate with a waiting time T_{wait} is denoted as $N(< T_{wait})$. The green points in Figure 7 illustrate the variation of $N(< T_{wait})$ with T_{wait} . In many cases, researchers often fit the $N(< T_{wait})$ vs. T_{wait} curve using a normalized Weibull distribution, defined as $W_{CDF}(\delta|k, r) = \exp[-(\delta r \Gamma(1 + 1/k))^k]$ (Oppermann et al. 2018), where the parameter $k \rightarrow 0$ converts the Weibull distribution into an exponential distribution. The blue dashed line in Figure 7 shows the Weibull distribution with coefficient $k = 0.84 \pm 0.02$ and burst rate $r = 8.01 \pm 0.15 \text{ hr}^{-1}$, indicating that the Weibull distribution is converging toward the exponential distribution. To further investigate this convergence, we also fit the $N(< T_{wait})$ vs. T_{wait} curve using a normalized exponential function, represented by the green dashed line in Figure 7. The reduced χ^2 values, which assess the goodness of fit, are unity for both the Weibull distribution (blue dashed line) and the normalized exponential function (red dashed line). We note that the arrival time of the bursts have been corrected using the Kaplan-Meier estimator (Kaplan & Meier 1958). In summary, the $N(< T_{wait})$ vs. T_{wait} curve is well-fitted by an exponential function, indicating that the 74 detected bursts

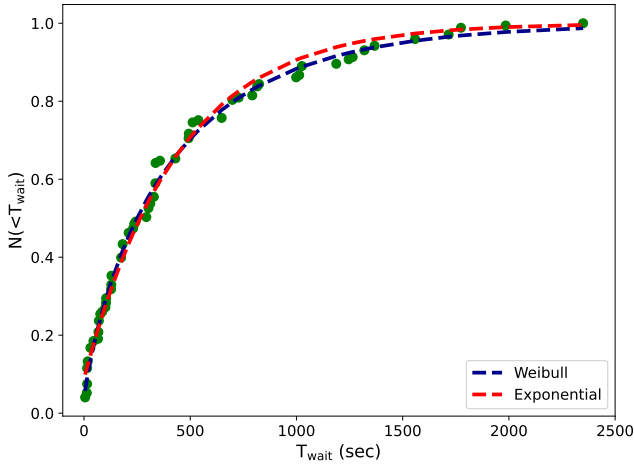


Figure 7. The normalized cumulative distribution ($N(<T_{\text{wait}})$) of the waiting time (T_{wait}) between consecutive bursts. The blue and red dashed lines are the fitting with a Weibull and an exponent function respectively.

from FRB 20180916B follow Poissonian statistics, suggesting that these bursts are non-clustered.

3.5. Burst Rate

Here we discuss the burst rate of FRB 20180916B depending on the 74 bursts detected at Band-3 of uGMRT. This discussion breaks into two parts. First, we discuss the variation of burst rate with phase and then the variation of cumulative burst rate with the fluence of the burst. We have estimated the burst rate, which is the number of bursts divided by the total observation duration, at each observation epoch separately and studied its variation with the median phase value for each epoch. Figure 8 shows the variation of burst rate (\mathcal{R}) with $\bar{\phi}$ at each of the observation epochs. We find that the variation of \mathcal{R} with $\bar{\phi}$ follows a particular characteristic where it peaks at the value of $\bar{\phi} = 0.54$. This implies that the burst rate of FRB 20180916B is maximum near the middle of its activity window. The green horizontal dashed line in figure 8 shows the average burst rate of FRB 20180916B considering all the observation epochs together. We find the value of the average burst rate is ~ 4 burst per hour at the observational frequency of 400 MHz with fluence values above 0.14 Jy ms. This is higher than the burst rates of this repeater reported by Chawla et al. (2020), Pleunis et al. (2021b), and Sand et al. (2022) (Table 3), which are 1.8 bursts per hour with fluence above 5 Jy ms at 600 MHz, 0.3 bursts per hour with fluence above 26 Jy ms at 150 MHz, and 0.7 bursts per hour with fluence above 0.5 Jy ms at 400 MHz (from an earlier uGMRT observation), respectively. The burst rate predicted from our observation is comparable to the rate reported by Sand et al. (2022) (Table 3),

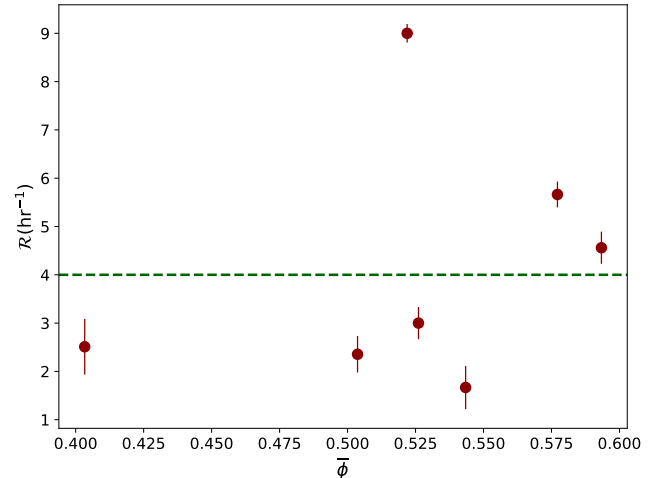


Figure 8. The variation of burst rate (\mathcal{R}) with the median value of activity phases ($\bar{\phi}$) of FRB 20180916B at each of the observation epochs. Here the error bars show the 1σ uncertainty in the estimation of \mathcal{R} and the green horizontal dashed line shows the burst rate averaged over all the observation epochs.

which is 4.2 bursts per hour with fluence above 0.2 Jy ms at 800 MHz. However, it is smaller than the burst rate reported by Bethapudi et al. (2023) (Table 3), which is 22.8 bursts per hour with fluence above 0.005 Jy ms at 6 GHz. We note that the Euclidean scaling from a fluence of 0.14 Jy ms to 0.005 Jy ms results in an increase in the burst rate from 4 to 18 bursts per hour, which is comparable to the burst rate reported by Bethapudi et al. (2023). It should also be noted that burst rate strongly depends on the observing frequency and the threshold fluence value of the telescope.

We now discuss the variation of the cumulative burst rate $\mathcal{R}_{\text{cum}}(> F_{\text{int}})$ with the intrinsic fluence F_{int} of the bursts from FRB 20180916B. This is defined as the number of bursts having an intrinsic fluence greater than F_{int} , divided by the observation time. We assessed the fluence completeness of all detected bursts using the method described in Keane & Petroff (2015).

Figure 9 shows the variation of the natural logarithmic value of the cumulative burst rate ($\ln \mathcal{R}_{\text{cum}}(> F_{\text{int}})$) with the natural logarithmic value of the intrinsic fluence ($\ln F_{\text{int}}$) for all 74 bursts from FRB 20180916B. The variation of $\ln \mathcal{R}_{\text{cum}}(> F_{\text{int}})$ vs. $\ln F_{\text{int}}$ is divided into three regions, namely R_0 , R_1 , and R_2 . In region R_0 , which includes bursts from this repeater with an intrinsic fluence value $F_{\text{int}} < 0.96$ Jy ms, all bursts are fluence incomplete and are therefore not considered for further modelling. In contrast, regions R_1 (0.96 Jy ms $< F_{\text{int}} < 2.45$ Jy ms) and R_2 ($F_{\text{int}} > 2.45$ Jy ms) contain fluence-complete bursts, which were used to model

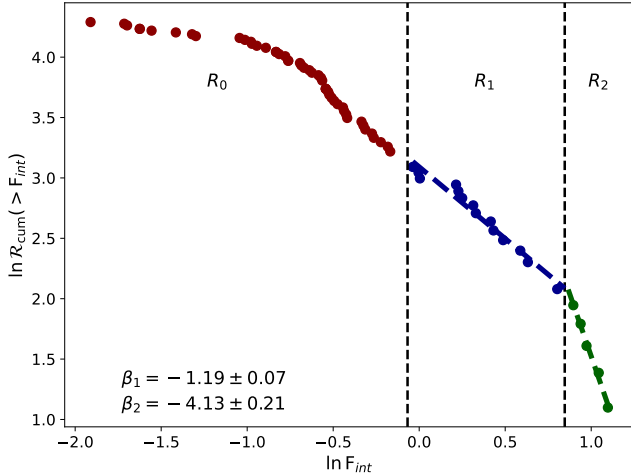


Figure 9. The variation of the natural logarithmic value of the cumulative burst rate ($\ln \mathcal{R}_{\text{cum}}$) with the natural logarithmic value of the intrinsic fluence ($\ln F_{\text{int}}$) emitted by the source.

the $\ln \mathcal{R}_{\text{cum}}(> F_{\text{int}})$ vs. $\ln F_{\text{int}}$ variation. We found that the fluence-complete bursts from FRB 20180916B can be fitted using a broken power law with indices $\beta_1 = -1.19 \pm 0.07$ for region R_1 and $\beta_2 = -4.13 \pm 0.21$ for region R_2 , with the break in intrinsic fluence located at 2.45 Jy ms. The reduced χ^2 value (which determines the goodness of fit) for this fitting is 0.98 (close to unity), and the fitted curves for both R_1 and R_2 are shown as dashed lines in Figure 9.

Previously, CHIME/FRB (2020) reported a power law modelling of the cumulative burst rate for FRB 20180916B with a single power law index of -3.3 . However, they did not identify any turnover in the distribution at lower fluences, likely due to the sensitivity limit of CHIME (400 – 800 MHz) or the intrinsic burst distribution. Later, Pastor et al. (2021) reported power law modelling of the cumulative burst rate for this repeater using the Apertif (1220 – 1520 MHz) telescope, identifying two turnovers. For $F > 7.8$ Jy ms, the power law index was -1.4 ± 0.1 ; for 3.2 Jy ms $< F < 7.8$ Jy ms, the index was -0.7 ± 0.1 ; and for $F < 3.2$ Jy ms, the index was -0.2 ± 0.1 . The studies mentioned above mainly probe the high fluence bursts from this repeater observed at relatively high frequencies. In contrast, our observations detected low intrinsic fluence bursts from FRB 20180916B at a low-frequency regime, showing a broken power law in its cumulative burst rate with power law indices that change sharply with the turnover of intrinsic fluence. Recently, Bethapudi et al. (2024) identified two fluence turnovers at 0.18 Jy ms and 1.10 Jy ms using 79 bursts from FRB 20180916B at uGMRT (550–750 MHz), with 0.18 Jy ms considered as the flu-

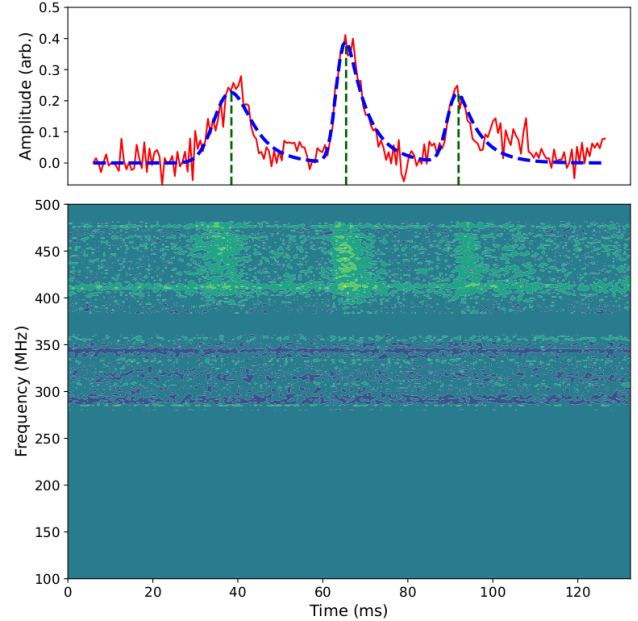


Figure 10. The dynamic spectrum and profile of a sub-burst structure from FRB 20180916B at an activity phase $\phi = 0.527$.

ence completeness limit. The reported power indices (Bethapudi et al. 2024) are -0.51 ± 0.01 for $F < 1.10$ Jy ms and -1.09 ± 0.07 for $F > 1.10$ Jy ms. However, they reported bursts with lower fluence values and relatively flatter power indices compared to our observations.

3.6. Quasi Periodicity

We previously discussed that we had detected 74 predominantly single-component bursts at Band-3 of uGMRT. Out of 74 bursts, we have found only a bursts where sub-bursts have been seen. Figure 10 shows a burst from FRB 20180916B with $\phi = 0.527$ has three sub-bursts with a separation of 29.5 ms indicating a quasi-periodicity of 29.5 ms.

Recently, Kramer et al. 2023 have shown a very intriguing relation between the period of quasi-periodic substructure and the rotational period of the neutron star which spans more than six orders of magnitude in the pulse period. To establish the above-mentioned relation, they considered the observed period of the quasi-periodic substructure (P_μ) of magnetars, RRATs and pulsars, and the corresponding rotational period of neutron stars (P). They found that P_μ connect with P through the relation $P_\mu = (0.94 \pm 0.04) \times P^{(0.97 \pm 0.05)}$ (Kramer et al. 2023), where P is in sec and P_μ is in ms. Using the above-mentioned relation, the authors estimated the rotation period of the neutron star (magnetar) assuming that magnetar is the source of FRB 20180916B, FRB 20201124A and FRB 20191221A, where they used the observed period of the quasi-

periodic substructure of these FRBs for this calculation. For FRB 20180916B, the average value of the period of the quasi-periodic substructure of the bursts was obtained from the detection of 28 bursts (Pastor et al. 2023) at Apertif (Pastor et al. 2021). Considering the quasi-periodicity obtained from our observations and the relation between P_μ and P (Kramer et al. 2023) discussed above we find out the rotational periods of neutron stars, which are $P = 34.9$ sec for $P_\mu = 29.5$ ms (figure 10).

3.7. Frequency Drifting

The time–frequency downward drifting pattern is a common characteristic of repeaters (Wang et al. 2019). Chawla et al. (2020); Pearlman et al. (2020); Sand et al. (2022); Trudu et al. (2023) reported linear drift rates for the bursts from FRB 20180916B as -4.2 MHz ms^{-1} , -6.6 MHz ms^{-1} , -8.0 MHz ms^{-1} , -9.7 MHz ms^{-1} , and -5.9 MHz ms^{-1} , using observations from GBT (300 – 400 MHz), LOFAR (110 – 188 MHz), GBT (600 – 1000 MHz), SRT (300 – 400 MHz), and uGMRT (300 – 500 MHz), respectively.

In contrast, we did not observe any linear drifting pattern in the dynamic spectra for the 74 bursts from this repeater, while most of the bursts detected in our observation are single-component in nature.

4. SUMMARY AND DISCUSSION

We conducted an interferometric observation of FRB 20180916B from November 26, 2020, to March 21, 2021, over seven different epochs, sampling the activity phase space of this repeater from $\phi = 0.4$ to $\phi = 0.6$. Simultaneous phased array observations were performed at Band-3 (250 – 500 MHz), Band-4 (550 – 850 MHz), and Band-5 (1060 – 1460 MHz) of uGMRT, covering a wide frequency range of 250 – 1460 MHz with a frequency resolution of approximately 48.83 kHz and a time resolution of 655.36 μs . In our observations, we detected 74 bursts at Band-3 and 4 bursts at Band-4, while no bursts were detected at Band-5. Additionally, we did not find any simultaneous detections of bursts

at both Band-3 and Band-4. In this paper, we focus solely on the 74 bursts detected at Band-3 to examine the variations in their physical parameters. We discuss the variations in the observed parameters of these 74 bursts with the activity phase of FRB 20180916B and compare our findings with existing literature on this repeater. The qualitative and quantitative nature of these physical parameter variations provides valuable insights for theoretical astrophysicists, helping to enhance the modeling of the source mechanism and the local environment of the FRB 20180916B.

Using this sample of 74 bursts in band-3 (250–500 MHz) and 4 bursts in band-4 (550–850 MHz), it was observed that the median peak frequency, along with the excess median dispersion measure and scattering, all reach their maximum values around the middle of the activity phase. This possibly indicates that the bursts encounter denser plasma closer to the centre of the activity window. This suggests an orbital motion (e.g. Lyutikov et al. 2020), with the activity window centred around the point of closest approach possibly involving interactions with a companion star or a stellar wind. The excess median dispersion measure at this point constrains the plasma density within the orbit, while the variation in the median peak frequency likely provides insights into the emission process itself. The estimated quasi-periodicity observed in the burst, indicating a neutron star rotation period of 35 seconds, supports the hypothesis of a long-period radio transient in a binary system as the progenitor of FRB 20180916B. Gaining a deeper understanding of its progenitor could offer valuable insights into the broader origins of FRBs.

ACKNOWLEDGEMENT

We acknowledge the support of the Department of Atomic Energy, Government of India, under project no. 12-R&D-TFR-5.02-0700. The GMRT is run by the National Centre for Radio Astrophysics of the Tata Institute of Fundamental Research, India. We acknowledge the support of GMRT telescope operators for observations. We appreciate the insightful inputs provided by Ujjwal Panda and Chahat Dudeja during FRB data analysis.

REFERENCES

- Andersen, B., Bandura, K., Bhardwaj, M., et al. 2019, The Astrophysical Journal Letters, 885, L24
- Bethapudi, S., Spitler, L., Li, D., et al. 2024, arXiv preprint arXiv:2409.12584
- Bethapudi, S., Spitler, L., Main, R., Li, D., & Wharton, R. 2023, Monthly Notices of the Royal Astronomical Society, 524, 3303

Table 2. The observed ranges of parameters of the bursts from FRB 20180916B using different telescopes are summarised here. The symbols DM , w_{int} , and τ represent the dispersion measure, intrinsic width, and scattering width respectively.

Telescope	Frequency	No. of	Phase	DM range	w_{int} range	τ range	Reference
Name	Range (MHz)	Bursts	Coverage	(pc cm^{-3})	(ms)	(ms)	
CHIME	400 – 800	38	–	348.8 – 350.1	0.58 – 8.60	–	CHIME/FRB 2020
Effelsberg	4000 – 8000	8	0.25 – 0.30	–	0.26 – 3.42	–	Bethapudi et al. 2023
GBT	300 – 400	8	0.47 – 0.57	348.7 – 349.5	1.50 – 5.89	1.80 – 5.90	Chawla et al. (2020)
CHIME	400 – 800	44	0.40 – 0.65	348.7 – 350.1	–	–	Mckinven et al. (2023)
Apertif	1220 – 1520	9	–	348.9 – 349.4	–	36.20 – 48.20	Pastor et al. (2021)
LOFAR	110 – 190	54	–	347.3 – 350.7	–	–	Pastor et al. (2021)
EVN	1636 – 1764	4	–	345.0 – 356.0	0.24 – 1.86	–	Marcote et al. (2020)
uGMRT	550 – 750	15	–	347.8 – 349.0	–	–	Marthi et al. (2020)
EVN	1636 – 1764	4	–	–	0.24 – 1.86	–	Nimmo et al. (2021)
CHIME	400 – 800	8	–	348.7 – 370.4	0.76 – 8.60	–	Pearlman et al. (2020)
LOFAR	110 – 188	18	0.53 – 0.79	–	42.00 – 119.00	46.69 – 54.14	Pleunis et al. (2021b)
GBT	600 – 1000	7	0.37 – 0.64	348.6 – 350.2	2.80 – 10.30	–	Sand et al. (2022)
uGMRT	300 – 500	4	0.37 – 0.64	348.6 – 350.2	2.46 – 8.40	1.67 – 2.51	Sand et al. (2022)
SRT	300 – 400	14	0.47 – 0.62	–	9.00 – 23.00	–	Trudu et al. (2023)
uGMRT	300 – 500	7	0.62 – 0.63	–	6.00 – 20.80	–	Trudu et al. (2023)
uGMRT	250 – 500	74	0.40 – 0.60	341.24 – 356.71	0.68 – 29.53	0.03 – 14.47	Current Analysis

Bhat, N. D. R., Cordes, J. M., Camilo, F., Nice, D. J., & Lorimer, D. R. 2004, *The Astrophysical Journal*, 605, 759

Braga, C., Cruces, M., Cassanelli, T., et al. 2024, arXiv preprint arXiv:2408.12567

Caleb, M., Stappers, B., Rajwade, K., & Flynn, C. 2019, *Monthly Notices of the Royal Astronomical Society*, 484, 5500

Chawla, P., Andersen, B., Bhardwaj, M., et al. 2020, *The Astrophysical Journal Letters*, 896, L41

CHIME/FRB. 2020, *Nature*, 582, 351

CHIME/FRB-Collaboration, Amiri, M., Andersen, B. C., Bandura, K., et al. 2021, *The Astrophysical Journal Supplement Series*, 257, 59

CHIME/FRB-Collaboration, Amiri, M., Andersen, B. C., et al. 2020, *Nature*, 582, 351

Connor, L., Miller, M., & Gardenier, D. 2020, *Monthly Notices of the Royal Astronomical Society*, 497, 3076

Deneva, J., Stovall, K., McLaughlin, M., et al. 2016, *The Astrophysical Journal*, 821, 10

Gajjar, V., Siemion, A., et al. 2018, *ApJ*, 863, 2

Gupta, Y., Ajithkumar, B., Kale, H. S., et al. 2017, *Current Science*, 707

Houben, L., Spitler, L., ter Veen, S., et al. 2019, *Astronomy & Astrophysics*, 623, A42

Kaplan, E. L., & Meier, P. 1958, *Journal of the American statistical association*, 53, 457

Keane, E. F., & Petroff, E. 2015, *Monthly Notices of the Royal Astronomical Society*, 447, 2852

Kramer, M., Liu, K., Desvignes, G., Karuppusamy, R., & Stappers, B. W. 2023, *Nature Astronomy*, 1

Kumar, P., Shannon, R., et al. 2019, *ApJL*, 887, L30

Lin, H.-H., Main, R., Pen, U.-L., et al. 2022, arXiv preprint arXiv:2208.13677

Lorimer, D. 2011, *Astrophysics Source Code Library*, ascl

Lorimer, D. R., & Kramer, M. 2005, *Handbook of pulsar astronomy*, Vol. 4 (Cambridge university press)

Lyutikov, M., Barkov, M. V., & Giannios, D. 2020, *The Astrophysical Journal Letters*, 893, L39

Marcote, B., Nimmo, K., et al. 2020, *Nature*, 577, 190

Marcote, B., Paragi, Z., Hessels, J., et al. 2017, *The Astrophysical Journal Letters*, 834, L8

Marthi, V. R., Gautam, T., Li, D., et al. 2020, *Monthly Notices of the Royal Astronomical Society: Letters*, 499, L16

Mckinven, R., Gaensler, B., Michilli, D., et al. 2023, *The Astrophysical Journal*, 950, 12

Nimmo, K., Hessels, J., Keimpema, A., et al. 2021, *Nature Astronomy*, 5, 594

Table 3. The observed range of parameters of the bursts from FRB20180916B using different telescopes is summarized here. The symbols S_ν , F and \mathcal{R} represent the flux density, fluence, and burst rate respectively.

Telescope	Frequency	No. of	S_ν range	F range	\mathcal{R} (hr^{-1})	Drift Rate	Ref
Name	Range (MHz)	Bursts	(Jy)	(Jy ms)	(> F Jy ms)	(MHz ms^{-1})	
CHIME	400 – 800	38	0.30 – 6.10	0.40 – 37.00	–	–	CHIME/FRB 2020
Effelsberg	4000 – 8000	8	0.18 – 1.84	0.08 – 1.49	22.8 (> 0.005)	–	Bethapudi et al. 2023
GBT	300 – 400	8	0.98 – 3.58	5.20 – 48.90	1.8 (> 22.0)	–4.2	Chawla et al. (2020)
CHIME	400 – 800	44	–	–	–	–	Mckinven et al. (2023)
Apertif	1220 – 1520	9	–	38.00 – 318.00	–	–	Pastor et al. (2021)
LOFAR	110 – 190	54	–	1.20 – 58.30	–	–6.6	Pastor et al. (2021)
EVN	1636 – 1764	4	0.50 – 2.30	0.20 – 2.53	–	–	Marcote et al. (2020)
uGMRT	550 – 750	15	0.17 – 23.65	0.09 – 47.80	–	–	Marthi et al. (2020)
EVN	1636 – 1764	4	–	0.20 – 2.53	–	–	Nimmo et al. (2021)
CHIME	400 – 800	8	0.40 – 6.10	0.40 – 16.30	–	–	Pearlman et al. (2020)
LOFAR	110 – 188	18	1.65 – 10.57	26.00 – 308.00	0.3 (> 26.0)	–	Pleunis et al. (2021b)
GBT	600 – 1000	7	0.12 – 4.39	0.24 – 6.10	4.2 (> 0.2)	–8.0	Sand et al. (2022)
uGMRT	300 – 500	4	0.43 – 6.92	1.49 – 7.20	0.7 (> 0.5)	–	Sand et al. (2022)
SRT	300 – 400	14	2.10 – 12.2	15.00 – 172.00	–	–9.7	Trudu et al. (2023)
uGMRT	300 – 500	7	0.20 – 7.90	0.60 – 7.90	–	–5.9	Trudu et al. (2023)
uGMRT	250 – 500	74	0.12 – 2.40	0.14 – 15.23	4.0 (> 0.14)	–	Current Analysis

Ocker, S. K., Cordes, J. M., Chatterjee, S., et al. 2022, The Astrophysical Journal, 931, 87

Oppermann, N., Yu, H.-R., & Pen, U.-L. 2018, Monthly Notices of the Royal Astronomical Society, 475, 5109

Ott, M., Witzel, A., Quirrenbach, A., et al. 1994, Astronomy and Astrophysics (ISSN 0004-6361), vol. 284, no. 1, p. 331-339, 284, 331

Pastor, Marazuela, I., Connor, L., van Leeuwen, J., et al. 2021, Nature, 596, 505

Pastor, Marazuela, I., Van Leeuwen, J., Bilous, A., et al. 2023, Astronomy & Astrophysics, 678, A149

Pearlman, A. B., Majid, W. A., Prince, T. A., et al. 2020, The Astrophysical Journal Letters, 905, L27

Petroff, E., Oostrum, L. C., Stappers, B. W., et al. 2019, Monthly Notices of the Royal Astronomical Society, 482, 3109

Pilia, M., Burgay, M., Possenti, A., et al. 2020, The Astrophysical Journal Letters, 896, L40

Pleunis, Z., Michilli, D., Bassa, C., et al. 2021a, The Astrophysical Journal Letters, 911, L3

—. 2021b, The Astrophysical Journal Letters, 911, L3

Rajwade, K., Mickaliger, M., et al. 2020, MNRAS, 495, 3551

Rajwade, K. M., & van Leeuwen, J. 2024, Universe, 10, 158

Ravi, V., Catha, M., D’Addario, L., et al. 2019, Nature, 572, 352

Sand, K. R., Faber, J. T., Gajjar, V., et al. 2022, The Astrophysical Journal, 932, 98

Trudu, M., Pilia, M., Nicastro, L., et al. 2023, Astronomy & Astrophysics, 676, A17

Wang, W., Zhang, B., Chen, X., & Xu, R. 2019, The Astrophysical Journal Letters, 876, L15

Zhang, B. 2023, Reviews of Modern Physics, 95, 035005